Jurnal
Teknologi

Full Paper

MECHANICAL CHARACTERIZATION OF POLYLACTIC ACID WITH DIFFERENT INFILL PATTERNS AND ARRANGEMENTS USING FUSED DEPOSITION MODELING

Nur Salwa Aliana Che Nordin, Liyana Tajul, Hasnulhadi Jaafar*, Nor Amalina Muhayudin, Khairul Salleh Basaruddin

Faculty of Mechanical Engineering and Technology, Universiti Malaysia Perlis, 02600, Arau, Perlis, Malaysia

Article history
Received
28 August 2025
Received in revised form
29 December 2025
Accepted
29 December 2025
Published Online
29 August 2026

*Corresponding author
hasnulhadi@unimap.edu.my

Graphical abstract

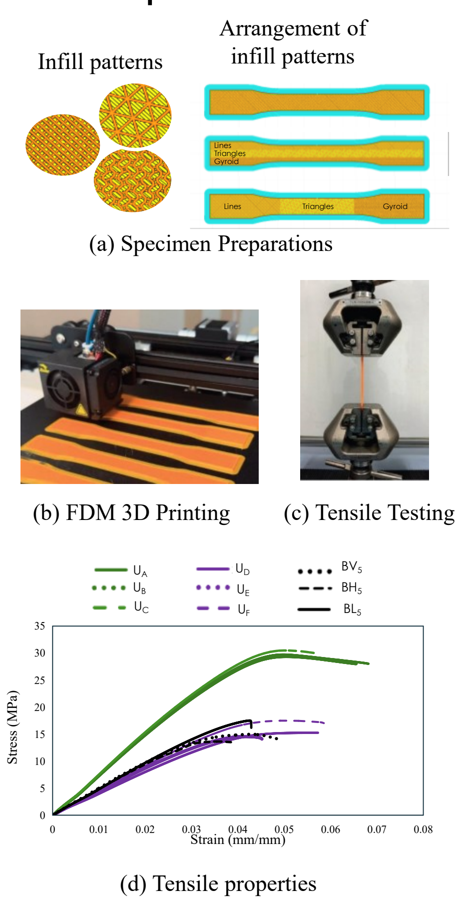

Abstract

Infill patterns significantly affect the mechanical properties, printing time and material consumption of 3-Dimensional (3D) printed Polylactic Acid (PLA) parts. Despite the wide variety of available infill patterns, the effect of combining and arranging multiple infill patterns on strength-to-weight ratio within a single print remains underexplored. This study investigates the effect of infill pattern arrangements on enhancing the strength-to-weight performance for applications requiring strong yet lightweight components. Three infill patterns (Lines, Triangles and Gyroid) were selected and arranged in three different configurations: by-layer, by-horizontal area and by-vertical area. By-layer arrangement exhibited improved tensile strength, Young's Modulus and strength-to-weight ratio. BL_5 with 50% infill density and arranged by-layer, demonstrated the best performance, with a tensile strength of 17.77 MPa and strength-to-weight ratios of 2.85 MPa/g. The infill patterns in this arrangement, delays crack propagation, as the non-continuous geometry created by the varied patterns disrupts the crack path. In contrast, the lowest tensile strength was observed for by-vertical area arrangement, where the tension load was applied perpendicular to the interface between different infill patterns, increasing the likelihood for crack initiation and propagation. Although the by-layer arrangement required a longer printing time, it produced part with a superior strength-to-weight ratio compared to the other arrangements, making it an effective strategy for balancing mechanical strength and material efficiency.

Keywords: Multiple Infill Patterns, Infill Arrangement, Strength-to-Weight Ratio, 3D Printing

Abstrak

Corak isian memberi kesan yang signifikan terhadap sifat mekanikal, masa pencetakan dan penggunaan bahan bagi komponen Asid Polilaktik (PLA) bercetak 3-Dimensi (3D). Walaupun terdapat pelbagai corak isian yang tersedia, kesan penggabungan dan susunan pelbagai corak isian terhadap nisbah kekuatan-kepada-berat dalam satu proses cetakan masih kurang diterokai. Kajian ini menyiasat kesan susunan corak isian dalam meningkatkan prestasi kekuatan-kepada-berat bagi aplikasi yang memerlukan komponen bersifat kuat tetapi ringan. Tiga corak isian (Lines, Triangles dan Gyroid) telah dipilih dan disusun dalam tiga konfigurasi berbeza, iaitu mengikut lapisan (by-layer), mengikut kawasan mendatar (by-horizontal area) dan mengikut kawasan menegak (by-vertical area). Susunan mengikut lapisan (by-layer) menunjukkan peningkatan dalam kekuatan tegangan, Modulus Young dan nisbah kekuatan-kepada-berat. Spesimen BL_5 dengan ketumpatan isian 50% yang disusun mengikut lapisan (by-layer) menunjukkan prestasi terbaik, dengan kekuatan tegangan sebanyak 17.77 MPa dan nisbah kekuatan-kepada-berat sebanyak 2.85 MPa/g. Corak isian dalam susunan ini didapati melambatkan rambatan retak kerana geometri tak selanjar yang terhasil daripada kepelbagaian corak mengganggu laluan retakan. Sebaliknya, kekuatan tegangan terendah diperhatikan bagi susunan mengikut kawasan menegak (by-vertical area), di mana beban tegangan dikenakan secara serenjang terhadap antara muka corak isian yang berbeza, sekali gus meningkatkan kebarangkalian permulaan dan rambatan retak. Walaupun susunan mengikut lapisan (by-layer) memerlukan masa pencetakan yang lebih lama, ia menghasilkan komponen dengan nisbah kekuatan-kepada-berat yang lebih unggul berbanding susunan lain, menjadikannya satu strategi yang berkesan untuk mengimbangi kekuatan mekanikal dan kecekapan penggunaan bahan.

Kata kunci: Pelbagai Corak Isian, Susunan Isian, Nisbah Kekuatan-kepada-Berat, Pencetakan 3D

1.0 INTRODUCTION

Additive manufacturing (AM) is commonly known as 3D printing, involves creating three-dimensional (3D) physical objects. The object is created by depositing material layer-upon-layer based on the Computer Aided Design (CAD) model. Unlike the traditional subtractive method, AM allows the production of objects with complex geometry quickly and at the same time reduces material waste [1-3]. Based on ISO/ASTM 52900:2021, AM technology is categorized into seven main groups, known as binder jetting, direct energy deposition, material extrusion, material jetting, powder bed fusion, sheet lamination and vat photopolymerization. Among these 3D printing groups, material extrusion is broadly adopted due to its cost effectiveness and user-friendly operation [4,5].

Fused Deposition Modeling (FDM) also referred to as Fused Filament Fabrication (FFF), is a widely used material extrusion-based 3D printing technology. In FDM, thermoplastic filament is fed into the nozzle from a spool of material, heated to a semi-molten state before being pushed through a nozzle and selectively deposited onto the build platform. The nozzle is designed to move in the x-y planes while the bed platform moves vertically in the z-plane according to the generated toolpath. This process provides operational simplicity, cost-effectiveness, and material flexibility in producing functional prototypes and end-use products. The filament used in FDM covers a wide variety of thermoplastic materials including Polylactic Acid (PLA), Acrylonitrile Butadiene Styrene (ABS) and Polyethylene Terephthalate Glycol (PETG), hence supporting the demand of different material obligations from multiple industries [6-9]. Medical grade filaments are employed in 3D printing to produce customized medical devices, for example a substitute for traditional cast used for immobilization of fractured or deformed limbs [10-11]. These cast and splints require sufficient tensile strength (greater than 20 MPa) to hold and protect the injured body area, preventing movement that could hinder the healing process [12]. Additionally, this immobilizer should be lightweight to improve comfort of the patient and promote faster recovery [12-13]. In the automotive industry, one of the main applications of AM is to reduce the components weight as to reduce the fuel consumption [14-15]. For lightweight application, 3D printed polymer based automotive components are replacing the use of conventional heavy metal [16-17]. However, replacing metal without proper design strategies, limits the overall application of polymer if strength requirement could not be achieved.

In FDM, process parameters play a crucial role in controlling the mechanical properties and the amount of material consumption during printing process [18-21]. Kumaresan *et al*. [22] reported that increasing the infill density creates an improved tensile performance as more material fills up the empty spaces in the internal structure creating greater bonding between layers. Although the increasing amount of material directly enhanced mechanical strength, interpreting the influence of infill pattern is more complex, as wide variety of predefined patterns are offered in the slicing software and the involvement of various printing parameters. Tanveer *et al*. [23] stacked different infill densities in the horizontal area arrangement and found that this arrangement exhibited better tensile strength than the specimens with uniform infill density. According to Ambati *et al*., the resistance to failure improves as the infill pattern orientation was aligned with direction of the tensile loading [24]. Certain patterns such as gyroid or concentric offer superior tensile strength especially at higher density (more than 50%) rather than lower infill percentages when compared to tri-hexagon and octet [25]. The continuous structure and no sharp corners found in gyroid and concentric patterns are favorable as they improved uniform load distribution and minimize stress concentration points. Nevertheless, introducing multiple infill patterns in a single component introduces additional structural heterogeneity, complicating the interpretation and prediction of mechanical behavior.

While the effects of individual parameters involving density and infill pattern have been extensively studied, combining different infill patterns with different arrangements requires further in-depth analysis as this approach has great potential to fabricate 3D print parts with excellent strength-to-weight ratio. Combining and arranging different infill patterns in a single part can optimize the amount of material being used, hence producing lightweight components without compromising mechanical strength. Therefore, this study investigated the effects of infill patterns (Lines, Triangles and Gyroid) and their arrangement (by-layer, by-horizontal area and by-vertical area) on tensile properties, weight and printing time. These arrangements were selected based on ease of design implementation, while the chosen infill pattern offer significant difference in the internal structure that could help with achieving component with enhanced mechanical properties and lightweight.

2.0 METHODOLOGY

The material used for this study is made of Polylactic Acid (PLA) having a density of 1.24 g/cm^3 and melts at a temperature of 210 ℃. The diameter of the spooled filament is 1.75 mm with a total weight of 1 kg. The color of the selected filament was orange, and the PLA filaments properties are shown in Table 1.

Table 1 Mechanical properties of PLA filaments

PLA	Properties
Density	1.24 g/cm^3
Tensile strength	50 MPa
Coefficient of thermal expansion	68µm/m-°C
Flexural strength	80 MPa

The infill pattern and infill arrangements are the main parameters investigated in this study. The infill patterns are the structure that forms inside a printed product or part. Infill patterns are usually non-visible as they are formed inside and covered by the outer shell. Nevertheless, this internal structure is crucial in improving the mechanical properties. Three infill patterns were selected for this study which are Lines, Triangles and Gyroid. These patterns differ significantly in geometry, homogeneity as well as empty spaces, hence affecting the internal structure of the printed parts. Figure 1 shows the patterns generated with 50% density. For the Lines infill pattern, each layer consists of parallel lines that alternate at 90° between layers. This pattern provides strength in two dimensions, prints relatively fast and uses less material. In the Triangle pattern, three lines intersect at 60° angles within a single layer forming a clear triangular mesh structure. This pattern can provide good bonding within the internal structure owing to high number of contact points between layers. The Gyroid pattern on the other hand, is characterized by its 3D continuous wavy pattern with near-isotropic strength. The complexity of Gyroid pattern requires longer printing time and higher material consumption.

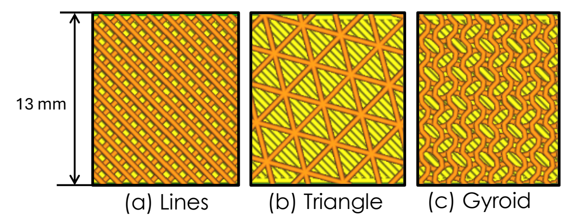

Figure 1 Selection of infill patterns with 50 % infill density

To investigate the effect of 3D-infill pattern distribution and their arrangement on mechanical performance, three distinct infill arrangements were employed in this study. The infill patterns (Lines, Triangles and Gyroid) as mentioned, were arranged in three distinct arrangements which are by-layer, by-horizontal area and by-vertical area. The arrangements shown in Figure 2 represent the most practical configurations for varying infill patterns within a single 3D-printed specimen. The specimen geometry was designed in accordance with the ASTM D638 Type I, a standard testing method for plastics to determine the tensile properties. For by-layer arrangement, the specimen was divided into three areas along the thickness direction (Z-axis). Each area was assigned to a different infill pattern consisting of either Lines, Triangles, or Gyroid. In by-horizontal area arrangement, the specimen was divided along its lengthwise direction, dividing the specimen into three regions, each with a width of 6.33 mm. Finally, in the by-vertical area arrangement, the specimen was segmented along its width into three sections which are left, center, and right. Like other arrangements, each section is filled with different infill patterns.

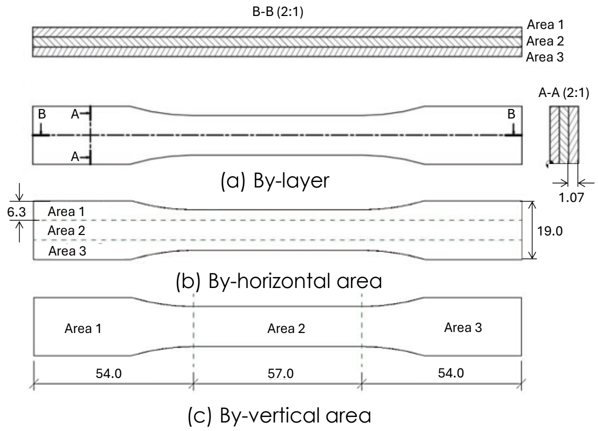

Figure 2 Infill pattern arrangement under three different configurations (in mm)

Table 2 summarizes the infill pattern and their arrangements applied in this study. Two sets of uniform infill pattern specimens were prepared with 50% (U_D, U_E and U_F) and 100% (U_A, U_B and U_C) infill densities. Each uniform specimen was fabricated using a single infill pattern (Lines, Triangles, or Gyroid), applied throughout the entire specimen. The uniform specimens served as control specimens providing baseline to evaluate the mechanical properties for specimens with different infill pattern arrangement. The remaining specimens contained varied infill patterns made from either Lines, Triangles, or Gyroid under different arrangements. The arrangements are by-layer (BL_1- BL_6), by-horizontal area (BH_1- BH_6), and by-vertical area (BV_1- BV_6). Each area was assigned a different infill pattern with a constant 50% density.

Table 2 Infill patterns and their arrangements

Type	Specimen	Infill Density	Area 1	Area 2	Area 3
Uniform (U)	U_A	100%	Lines	Lines	Lines
	U_B	100%	Triangles	Triangles	Triangles
	U_C	100%	Gyroid	Gyroid	Gyroid
Uniform (U)	U_D	50%	Lines	Lines	Lines
	U_E	50%	Triangles	Triangles	Triangles
	U_F	50%	Gyroid	Gyroid	Gyroid
(i) By-layer (BL) (ii) By-horizontal area (BH) (iii) By-vertical area (BV)	BL_1, BH_1, BV_1	50%	Lines	Triangles	Gyroid
	BL_2, BH_2, BV_2	50%	Triangles	Gyroid	Lines
	BL_3, BH_3, BV_3	50%	Gyroid	Lines	Triangles
	BL_4, BH_4, BV_4	50%	Gyroid	Triangles	Lines
	BL_5, BH_5, BV_5	50%	Lines	Gyroid	Triangles
	BL_6, BH_6, BV_6	50%	Triangles	Lines	Gyroid

The workflow for the 3D printing process is illustrated in Figure 3. The 3D model of the specimens was created using Autodesk Inventor, a 3D modeling software. The CAD model was then converted into STL format, a format that is compatible with most slicing software and 3D printers. The STL file was then sliced into layers using UltiMaker Cura slicing software before generating the corresponding toolpaths for 3D printing process. Printing parameters including layer height, layer thickness and build orientation were configured as shown in Table 3 to ensure good quality defect free prints. The nozzle temperature, bed temperature and layer thickness influence inter-layer bonding and subsequently affect the tensile strength and Young's Modulus. Therefore, these parameters were held constant to ensure that variations in tensile properties are attributed primarily to specimen configuration rather than process-induced variability. Figure 4 shows the sliced model of specimen sample 1 with varying infill pattern and arrangements. The slicer produced G-code instructions, which were then transferred to the Creality Ender 5 series FDM 3D printer for printing process.

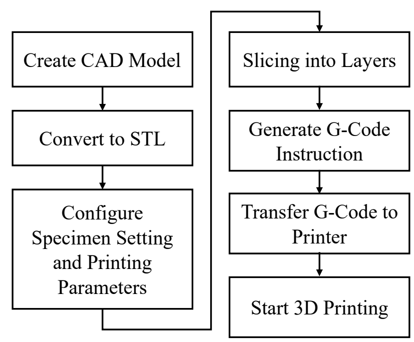

Figure 3 Workflow for the 3D printing process

Table 3 Constant printing parameters

Parameter	Value
Build orientation (degree)	Flat side 0°
Nozzle diameter (mm)	0.4
Filament diameter (mm)	1.75
Layer thickness (mm)	0.4
Nozzle temperature (°C)	210
Bed temperature (°C)	60

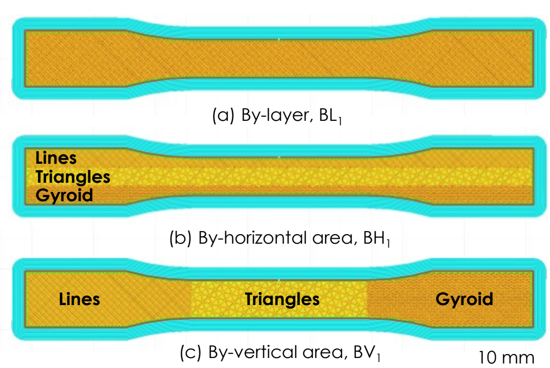

Figure 4 Sliced model with varying infill pattern and arrangements

The tensile properties of the printed specimens were tested using a Shimadzu 50 kN Universal Testing Machine (UTM). The test was conducted at a crosshead speed of 5 mm/min. Each sample was securely gripped at both ends, applied a uniaxial tensile load and gradually pulled in lengthwise direction until fracture. Each specimen was tested five times, with a total of 120 specimens being evaluated in this study.

3.0 RESULTS AND DISCUSSION

The specimens after tensile testing are shown in Figure 5. The tensile fracture results demonstrated that both infill density and pattern arrangement significantly influence the tensile behavior of the printed specimen. U_A, U_B and U_C fabricated with uniform infill pattern and 100% infill density exhibited similar fracture pattern. Reducing the infill density by 50% (U_D, U_E and U_F) led to earlier failure and more irregular crack paths, displaying an overall reduction in strength. Specimens under the proposed arrangements (BL, BH, BV), show that fracture consistently occurred within the gauge length. Specimens with the by-vertical area arrangement (BV) exhibited fracture localized in the region of interfaces between adjacent patterns indicating a weak interfacial bonding for this arrangement.

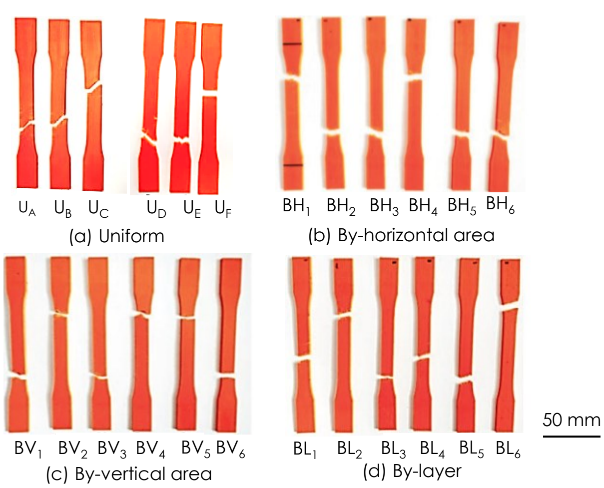

Figure 5 Specimen after tensile testing

Table 4 shows the effect of infill patterns and their arrangement type (uniform, by-layer, by-horizontal area and by-vertical area) on tensile properties. The mean and standard deviation values of tensile strength and Young's Modulus were obtained from five repeated tests per specimen. The standard deviation values recorded were relatively low (0.07–0.76 MPa for tensile strength and 3.40–13.90 MPa for Young's Modulus), indicating consistent mechanical behavior and good repeatability of the printing and tensile testing processes. The summary of the stress strain relationship for each arrangement of BL_5, BH_5 and BV_5 is shown in Figure 6. Uniform infill with 100% density for U_A, U_B and U_C, achieved the highest tensile strengths between 29.39 to 30.52 MPa (refer to Figure 7), and strength-to-weight ratios between 3.31 to 3.43 MPa/g (refer to Figure 8). The 50% uniform infill pattern shows a significant decrement in the tensile strength readings (14.55–17.33 MPa). For both 50% and 100% uniform infill pattern, Gyroid shows the highest tensile strength. Gyroid continuous curve structure helps distribute stress and forces more evenly when compared to line and triangle patterns. The unique Gyroid interlocking lattice structure further enhances strength and structural integrity.

Table 4 Tensile properties of printed specimen

Type	Specimen	Tensile Strength (MPa) (SD)	Young's Modulus (MPa) (SD)	Strength-to-Weight Ratio (MPa/g)
Uniform	U_A	29.81 (0.62)	757.13 (13.90)	3.35
	U_B	29.39 (0.61)	740.54 (12.37)	3.31
	U_C	30.52 (0.76)	773.38 (18.87)	3.43
	U_D	15.23 (0.60)	432.33 (13.22)	2.53
	U_E	14.55 (0.40)	398.55 (10.19)	2.44
	U_F	17.33 (0.19)	456.29 (7.83)	2.89
By-Horizontal Area	BH_1	14.79 (0.24)	470.33 (5.54)	2.39
	BH_2	15.35 (0.40)	501.87 (5.84)	2.55
	BH_3	13.90 (0.22)	458.00 (2.58)	2.32
	BH_4	14.32 (0.45)	496.26 (10.58)	2.34
	BH_5	14.74 (0.24)	485.15 (5.22)	2.46
	BH_6	14.63 (0.43)	486.26 (10.82)	2.39
By-Vertical Area	BV_1	13.50 (0.12)	481.78 (10.93)	2.25
	BV_2	13.77 (0.18)	486.90 (7.96)	2.31
	BV_3	14.02 (0.07)	477.32 (6.95)	2.33
	BV_4	13.30 (0.12)	484.97 (6.42)	2.25
	BV_5	14.67 (0.16)	505.57 (3.40)	2.44
	BV_6	13.37 (0.25)	485.90 (6.44)	2.23
By-Layer	BL_1	16.21 (0.62)	483.15 (5.90)	2.56
	BL_2	17.26 (0.39)	492.88 (3.77)	2.79
	BL_3	17.59 (0.44)	486.54 (7.30)	2.8
	BL_4	17.00 (0.24)	497.39 (6.01)	2.74
	BL_5	17.77 (0.24)	516.00 (11.90)	2.85
	BL_6	16.57 (0.49)	485.89 (5.35)	2.64

For 50% density, by-layer performed the best when compared to uniform, by-horizontal area and by-vertical area, with tensile strengths ranging from 16.21–17.77 MPa and strength-to-weight ratios up to 2.85 MPa/g. BL_5 exhibited the highest tensile strength among all specimen with 50% density, exceeding the specimen made of uniform single pattern (U_D, U_E and U_F). This shows that alternating patterns in the thickness direction enhance load distribution and delay fracture initiation. Tanveer *et al*. [23] found a similar trend in which different arrangement of infill structure improves the tensile strength due to increased resistance to crack propagation. The highest strength-to-weight ratio was found for uniform Gyroid infill pattern, U_F (2.89 MPa/g) closely followed by BL_5 of by-layer arrangement (2.85 MPa/g). Figure 9 shows the layers where two different patterns are connected for BL_5 (by-layer arrangement). The smooth transition between alternating patterns increases the contact area and bonding strength between filaments of adjacent layers. Furthermore, the change in pattern interrupts crack growth hence delays failure when adopting by-layer arrangement. In contrast, cracks can easily propagate in uniform patterns as lower resistance is introduced.

By-vertical area arrangement had the lowest tensile strength values overall of 13.30–14.67 MPa and the lowest strength-to-weight ratios (2.23–2.44 MPa/g). When tension load is applied perpendicular to the interface, the bonding strength and load-bearing efficiency weaken. The interface where different patterns connect (by-vertical area arrangement as shown in Figure 10(a)) creates the weakest region due to discontinuity of geometry that reduces mechanical interlocking. By-horizontal area arrangement shows moderate performance, but its tensile strength is lower compared to the uniform pattern. The interfaces which occur in the specimen length direction as illustrated in Figure 10(b), eliminate the weakest region as observed on by-vertical area. Nevertheless, the tensile strength is much lower than that of by-layer arrangement which might be due to the reduced contact area and bonding strength at the interface between patterns. The poor contact between the interfaces increases stress concentration points.

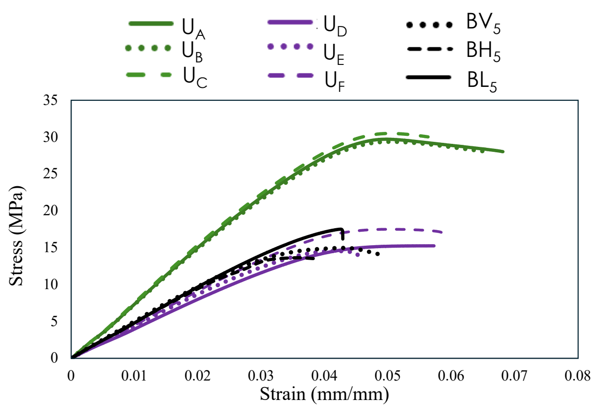

Figure 6 Stress strain relationship for infill pattern under different arrangements

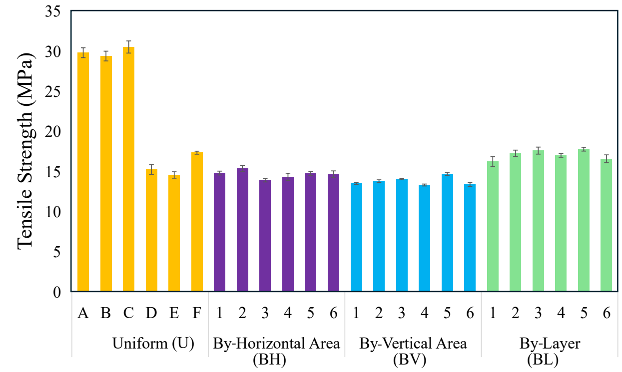

Figure 7 Tensile strength for different infill patterns and arrangements

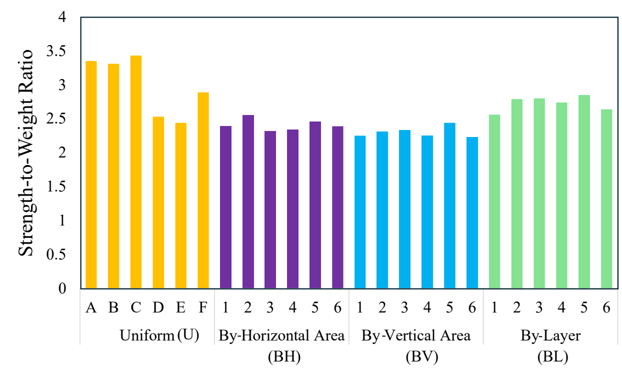

Figure 8 Strength-to-weight ratio for different infill patterns and arrangements

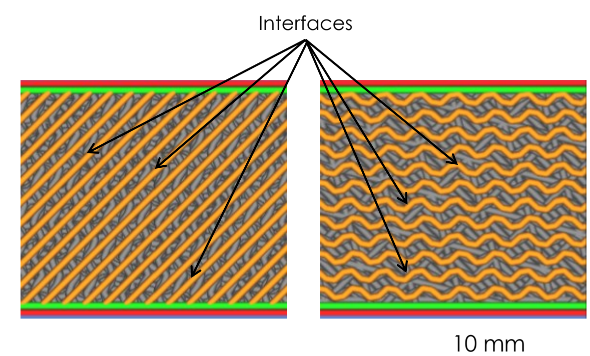

(a) Interfaces of gyroid (grey) and lines (orange)

(b) Interfaces of triangles (grey) and gyroid (orange)

Figure 9 Pattern interfaces for BL_5

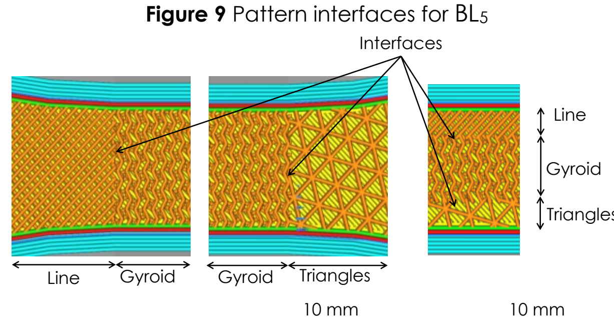

(a) By-vertical area

(b) By-horizontal area

Figure 10 Pattern interfaces for (a) BV_5 and (b) BH_5

The Young's modulus depicted in Figure 11 displayed a trend like the tensile strength, with the uniform arrangement for U_A, U_B and U_C at 100% infill density attaining the highest stiffness values, ranging from 740.54–773.38 MPa. The increased amount of material continuity reduces the void or empty spaces inside the specimen and therefore enhances the material's ability to resist elastic deformation. In contrast, U_D, U_E and U_F at 50% infill density displayed substantially lower stiffness (398.55–456.29 MPa) due to reduction in internal structure and increased in empty spaces. This observation is consistent with previous findings, which report that the presence of these empty spaces creates stress concentration regions, leading to increased flexibility and reduced resistance to deformation [26]. Both by-horizontal area and by-vertical area arrangements recorded an increased in the stiffness values, generally between 458.00–505.57 MPa. The by-layer arrangement exhibited higher modulus values (483.15–516.00 MPa) than the other 50% infill arrangement, suggesting that alternating layered structure improves load transfer between adjacent layers, thereby enhancing stiffness. Nevertheless, varying the arrangement of infill pattern under any configuration with 50% infill density shows an enhancement in the modulus of elasticity when compared to uniform arrangement.

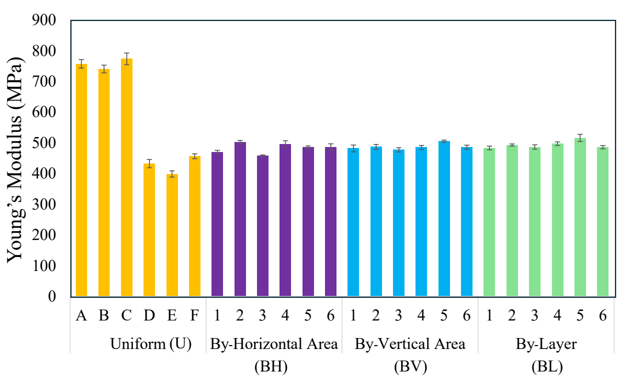

Figure 11 Young's modulus for different infill patterns and arrangements

Table 5 and Figure 12 show the printing time for each sample for different infill pattern arrangements. For uniform infill pattern with 100% infill density, the printing time is the same because the infill became fully solid for all patterns. For 50% density, Gyroid requires longer printing time due to its geometry complexity. By-layer arrangement at 50% density recorded the highest printing times as compared to other types of arrangement. The changing from one infill pattern to another consumes additional printing time as it may be caused by recalculation of the toolpaths that can result from more nozzle retractions, repositioning, and re-priming for each pattern change. Nonetheless, arrangement by-layer gives among the highest tensile strength (16.21–17.77 MPa) when comparing to 50% infill density group. In contrast, for uniform arrangement, a single infill pattern is repeated throughout the print, hence the nozzle follows a consistent, optimized path with less interruption. Still, even with the rise of printing time for by-horizontal area and by-layer arrangements, the weight for the 50% infill pattern remains almost constant across all prints as depicted in Figure 13. These findings suggested that the printing time is not proportionally related to material consumption. Pattern complexity and transition between the different patterns can significantly contribute to the overall printing time.

Table 5 Printing time and weight

Type	Specimen	Printing Time (min)	Weight (g) (SD)
Uniform	U_A	34.8	8.89 (0.02)
	U_B	34.8	8.89 (0.02)
	U_C	34.8	8.90 (0.04)
	U_D	26.8	6.02 (0.03)
	U_E	25.6	5.96 (0.02)
	U_F	47	6.06 (0.01)
By-Horizontal Area	BH_1	36.8	6.19 (0.03)
	BH_2	37.6	6.03 (0.06)
	BH_3	34	5.99 (0.01)
	BH_4	35.6	6.12 (0.12)
	BH_5	37.6	6.00 (0.04)
	BH_6	34	6.11 (0.03)
By-Vertical Area	BV_1	31.6	6.00 (0.03)
	BV_2	30	5.96 (0.03)
	BV_3	31.6	6.01 (0.02)
	BV_4	31.4	5.91 (0.02)
	BV_5	30.2	6.01 (0.06)
	BV_6	31.4	5.98 (0.01)
By-Layer	BL_1	48.2	6.33 (0.02)
	BL_2	47	6.19 (0.01)
	BL_3	47.8	6.29 (0.01)
	BL_4	47.8	6.20 (0.01)
	BL_5	47	6.23 (0.02)
	BL_6	48.2	6.28 (0.02)

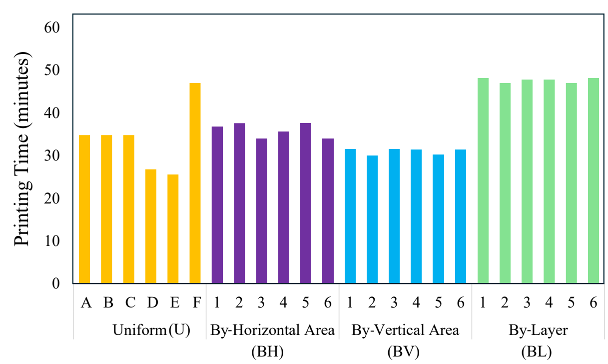

Figure 12 Printing time for different infill patterns and arrangements

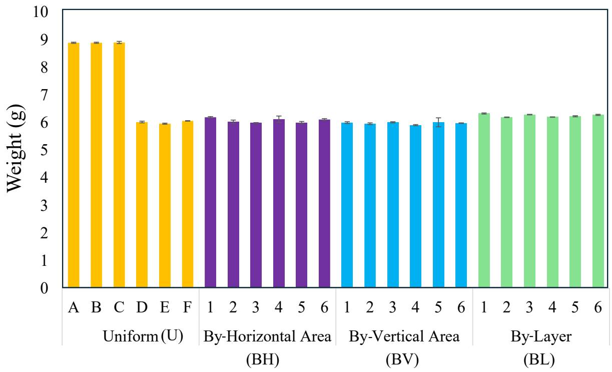

Figure 13 Weight of specimen for different infill patterns and arrangements

Figure 14 shows the microstructure of the fractured interface of the tensile specimen obtained for BH_5, BV_5 and BL_5 under three different arrangements with 50% infill density. These images were captured using a scanning electron microscope (SEM) S-3000N Hitachi at an acceleration of 5 KV in high vacuum mode.

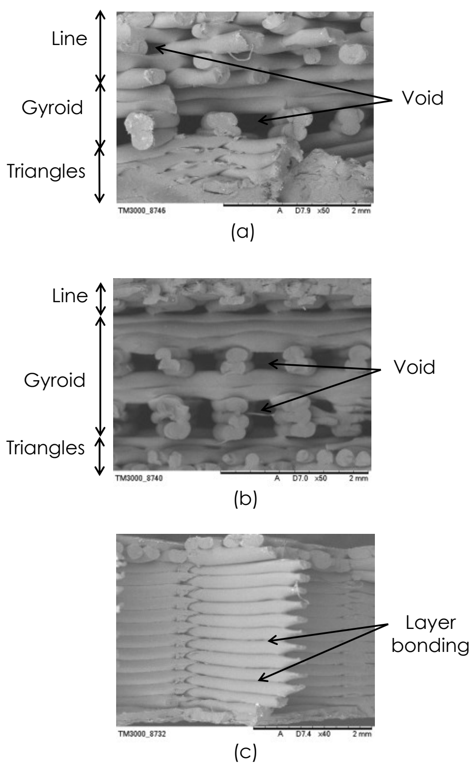

Figure 14 SEM images after tensile testing under different infill pattern arrangements; (a) BL_5, (b) BH_5 and (c) BV_5

The distinct patterns in Figure 14(a) observed for by-layer arrangement displayed a smoother transition between patterns. This smooth transition increases the overlapping contacts area creating a stronger bond and improved load transfer capability compared to other arrangements. Hence resulting in a higher tensile strength and stiffness. Meanwhile, the stacked configuration of Lines, Gyroid and Triangles patterns for by-horizontal arrangement shown in Figure 14(b) introduces discontinuity in the interfaces between patterns and creates additional voids formation. These discontinuities act as stress concentrators and produce weak interfaces that reduce bonding efficiency. These factors lower the tensile strength of this arrangement compared to the by-layer arrangement. For by-vertical area arrangement, fracture occurs within the Triangles pattern specifically at the nodes connecting the lines, where stress concentration was the highest (refer to Figure 14(c)). The larger empty spaces generated for Triangles pattern as shown in Figure 1, and the weak interface bonding reduces the structural integrity of the specimen.

4.0 CONCLUSION

This investigation demonstrates that in genera the infill geometry and architectural arrangement highly influenced the tensile behavior, elastic modulus, and failure modes of fused deposition modeling (FDM) components. The continuous wavy architecture of the Gyroid pattern of 50% uniform density exhibited superior characteristics and performance in tensile strength, Young's Modulus, and strength-to-weight ratio over conventional Lines and Triangles profiles. These outcomes were found due to its near-isotropic load distribution. However, multi-pattern hybridization surpassed uniform baselines, with the by-layer (BL5) arrangement recording the highest absolute tensile strength and optimal strength-to-weight performance. This improvement is attributed to the smooth transitional interface between pattern layers, which enhances inter-layer contact area and interfacial bond strength. in addition, localized pattern variation consistently yielded a higher modulus of elasticity compared to equivalent single-pattern configurations.

Conversely, discrete spatial interfaces shown structural vulnerabilities, as evidenced by the severe mechanical degradation observed in by-vertical arrangements. Geometric discontinuities at pattern boundaries impacted mechanical interlocking by concentrating stress along the nodal junctions of the Triangles geometry. Thus, this phenomenon creates premature structural failure. These findings provided clear design guidelines for optimum density infill to pattern arrangement combinations for superior strength-to-weight efficiency. Although by-layer arrangement requires longer printing times compared to other arrangements, the enhanced strength-to-weight ratio justifies the increased build time for load-bearing applications, whereas by-horizontal and by vertical arrangements provide faster printing strategies that are preferable for cost-effective or high-volume applications.

Conflicts of Interest

The authors declare that there is no conflict of interest regarding the publication of this paper.

References

[1] Zhou, L., J. Miller, J. Vezza, M. Mayster, M. Raffay, Q. Justice, Z. Al Tamimi, G. Hansotte, L. D. Sunkara, and J. Bernat. 2024. Additive Manufacturing: A Comprehensive Review. *Sensors*. 24(9): 2668. https://doi.org/10.3390/s24092668.

[2] Segovia-Guerrero, L., N. Baladés, J. J. Gallardo-Galán, A. J. Gil-Mena, and D. L. Sales. 2025. Additive vs. Subtractive Manufacturing: A Comparative Life Cycle and Cost Analyses of Steel Mill Spare Parts. *Journal of Manufacturing and Materials Processing*. 9(4): 138. https://doi.org/10.3390/jmmp9040138.

[3] Jung, S., L. B. Kara, Z. Nie, T. W. Simpson, and K. S. Whitefoot. 2023. Is Additive Manufacturing an Environmentally and Economically Preferred Alternative for Mass Production? *Environmental Science & Technology*. 57(16): 6373–6386. https://doi.org/10.1021/acs.est.2c04927.

[4] Raja, S., and A. John Rajan. 2023. Challenges and Opportunities in Additive Manufacturing Polymer Technology: A Review Based on Optimization Perspective. *Advances in Polymer Technology*. 2023: 8639185. https://doi.org/10.1155/2023/8639185.

[5] Tümer, E. H., and H. Y. Erbil. 2021. Extrusion-Based 3D Printing Applications of PLA Composites: A Review. *Coatings*. 11(4): 390. https://doi.org/10.3390/coatings11040390.

[6] Altıparmak, S. C., V. A. Yardley, Z. Shi, and J. Lin. 2022. Extrusion-Based Additive Manufacturing Technologies: State of the Art and Future Perspectives. *Journal of Manufacturing Processes*. 83: 607–636. https://doi.org/10.1016/j.jmapro.2022.09.032.

[7] Foorginejad, A., K. Kalili, V. Abdollahi, and H. Afshari. 2026. "Multi-Objective Optimization of Biomedical Scaffold Geometries for Mechanical and Porous Performance Enhancement. *International Journal of Engineering, Transactions A: Basics*. 39(1): 176–191. https://doi.org/10.5829/ije.2026.39.01a.14.

[8] Sri, H. A., and K. C. Vikram. 2021. Fused Deposition Modeling of an Aircraft Wing Using Industrial Robot with Non-Linear Tool Path Generation. *International Journal of Engineering, Transactions A: Basics*. 34(1): 272–282. https://doi.org/10.5829/ije.2021.34.01a.30.

[9] Sotov, A., A. Abdrakhmanova, A. Zaytsev, and A. Popovich. 2026. Bio-Inspired Continuously Reinforced Polymer Composites: Synthesis of Nature and Additive Manufacturing. *International Journal of Engineering*. 39(3): 770–788. https://doi.org/10.5829/ije.2026.39.03c.16.

[10] Lazzeri, S., E. Talanti, S. Basciano, R. Barbato, F. Fontanelli, F. Uccheddu, M. Servi, Y. Volpe, L. Vagnoli, E. Amore, *et al*. 2022. 3D-Printed Patient-Specific Casts for the Distal Radius in Children: Outcome and Pre-Market Survey. *Materials*. 15(8): 2863. https://doi.org/10.3390/ma15082863.

[11] Calderone, D., G. Cesarelli, C. Ricciardi, F. Amato, and F. Clemente. 2024. 3D Printing Application for Orthopedic Pediatric Surgery—A Systematic Review. *Rapid Prototyping Journal*. 30(11): 276–288. https://doi.org/10.1108/RPJ-05-2024-0222.

[12] Ekanayake, C., J. C. P. H. Gamage, P. Mendis, and P. Weerasinghe. 2023. Revolution in Orthopedic Immobilization Materials: A Comprehensive Review. *Heliyon*. 9(3): e13640. https://doi.org/10.1016/j.heliyon.2023.e13640.

[13] Patel, P., and P. Gohil. 2022. Custom Orthotics Development Process Based on Additive Manufacturing. *Materials Today: Proceedings*. 59(3): A52–A63. https://doi.org/10.1016/j.matpr.2022.04.858.

[14] Yang, J., B. Li, J. Liu, Z. Tu, and X. Wu. 2024. Application of Additive Manufacturing in the Automobile Industry: A Mini Review. *Processes*. 12(6): 1101. https://doi.org/10.3390/pr12061101.

[15] Böckin, D., and A. M. Tillman. 2019. Environmental Assessment of Additive Manufacturing in the Automotive Industry. *Journal of Cleaner Production*. 226: 977–987. https://doi.org/10.1016/j.jclepro.2019.04.086.

[16] Mohseni, Y., M. Mohseni, S. Suresh, M. Riotto, A. Jaggessar, J. P. Little, M. L. Wille, and P. K. Yarlagadda. 2023. Investigating Impacts of FDM Printing Parameters and Geometrical Features on Void Formation in 3D Printed Automotive Components. *Materials Today: Proceedings*.. In Press. https://doi.org/10.1016/j.matpr.2023.06.078.

[17] Mohanavel, V., K. A. Ali, K. Ranganathan, J. A. Jeffrey, M. M. Ravikumar, and S. J. Rajkumar. 2021. The Roles and Applications of Additive Manufacturing in the Aerospace and Automobile Sector. *Materials Today: Proceedings*. 47: 405–409. https://doi.org/10.1016/j.matpr.2021.04.596.

[18] Tanveer, M. Q., G. Mishra, S. Mishra, and R. Sharma. 2022. Effect of Infill Pattern and Infill Density on Mechanical Behaviour of FDM 3D Printed Parts—A Current Review. *Materials Today: Proceedings*. 62: 100–108. https://doi.org/10.1016/j.matpr.2022.02.310.

[19] Khan, I., M. Tariq, M. Abas, M. Shakeel, F. Hira, A. Al Rashid, and M. Koç. 2023. Parametric Investigation and Optimisation of Mechanical Properties of Thick Tri-Material Based Composite of PLA-PETG-ABS 3D-Printed Using Fused Filament Fabrication. *Composites Part C: Open Access*. 12: 100392. https://doi.org/10.1016/j.jcomc.2023.100392.

[20] Kumaresan, R., K. Kadirgama, M. Samykano, W. S. Harun, A. Thirugnanasambandam, and K. Kanny. 2025. In-Depth Study and Optimization of Process Parameters to Enhance Tensile and Compressive Strengths of PETG in FDM Technology. *Journal of Materials Research and Technology*. 37: 397–416. https://doi.org/10.1016/j.jmrt.2025.06.013.

[21] Haque, M. M., S. R. Dhrubo, A. F. Pranto, A. Ahmed, M. M. Arefin, M. Arifuzzaman, and M. S. Islam. 2025. Impact of Process Parameters and Material Selection on the Mechanical Performance of FDM 3D-Printed Components. *Hybrid Advances*. 100502. https://doi.org/10.1016/j.hybadv.2025.100502.

[22] Kumaresan, R., A. Kottasamy, J. Mogan, L. Sandanamsamy, M. Samykano, K. Kadirgama, and W. S. Harun. 2024. Preliminary Investigation on the Tensile Properties of FDM Printed PLA/Copper Composite. *Materials Today: Proceedings*. 109: 87–92. https://doi.org/10.1016/j.matpr.2023.10.054.

[23] Tanveer, M. Q., A. Haleem, and M. Suhaib. 2019. Effect of Variable Infill Density on Mechanical Behaviour of 3-D Printed PLA Specimen: An Experimental Investigation. *SN Applied Sciences*. 1(12): 1701. https://doi.org/10.1007/s42452-019-1744-1.

[24] Ambati, S. S., and R. Ambatipudi. 2022. Effect of Infill Density and Infill Pattern on the Mechanical Properties of 3D Printed PLA Parts. *Materials Today: Proceedings*. 64: 804–807. https://doi.org/10.1016/j.matpr.2022.05.312.

[25] Al Rashid, A., and M. Koç. 2025. 3D-Printed Recycled Polyethylene Terephthalate (PET) Sandwich Structures—Influence of Infill Design and Density on Tensile, Dynamic Mechanical, and Creep Response. *International Journal of Lightweight Materials and Manufacture*. In Press. https://doi.org/10.1016/j.ijlmm.2025.03.001.

[26] Khaliq, J., D. R. Gurrapu, and F. Elfakhri. 2023. Effects of Infill Line Multiplier and Patterns on Mechanical Properties of Lightweight and Resilient Hollow Section Products Manufactured Using Fused Filament Fabrication. *Polymers* 15: 2585. https://doi.org/10.3390/polym15122585.